Development of a deep learning-based model to diagnose mixed-type gastric cancer accurately

Xinjie Ning[1#], Ruide Liu[2#], Nan Wang[1], Xuewen Xiao[2], Siqi Wu[1], Yu Wang[3], Chenju Yi[1,4,5*]
Yulong He[1*], Dan Li[2*], Hui Chen[6]

1. Research Center, The Seventh Affiliated Hospital of Sun Yat-sen University, Shenzhen, 518107, China;
2. Department of Pathology, The First Affiliated Hospital of Gannan Medical University, Ganzhou, 341000, China;
3. Department of Respiratory Diseases, Central Medical Branch of PLA General Hospital, Beijing, 100081, China;
4. Shenzhen Key Laboratory of Chinese Medicine Active substance screening and Translational Research, Shenzhen, 518107, China;
5. Guangdong Provincial Key Laboratory of Brain Function and Disease, Guangzhou, 510080, China;
6. School of Life Sciences, Faculty of Science, University of Technology Sydney, Ultimo, NSW 2007, Australia.

# The authors contributed equally.
*Correspondence
Associate Professor Chenju Yi
E-mail: yichj@mail.sysu.edu.cn
Address: 628 Zhenyuan Road, Guangming, Shenzhen, Guangdong 518107, P.R. China.

Professor Yulong He
Email: heyulong@sysush.com
Address: 628 Zhenyuan Road, Guangming, Shenzhen, Guangdong 518107, P.R. China.

Dr. Dan Li
Email: lidanyy@126.com
Address: No. 128, Jinling Road, Ganzhou, Jiangxi 341000, P.R. China.

Abstract

Objective: The accurate diagnosis of mixed-type gastric cancer from pathology images presents a formidable challenge for pathologists, given its intricate features and resemblance to other subtypes of gastric cancer. Artificial Intelligence has the potential to overcome this hurdle. This study aimed to leverage deep machine learning techniques to establish a precise and efficient diagnostic approach for this cancer type which can also predict the metastatic risk using two software, QuPath and U-Net, which have not been trialled in gastric cancers.

Methods: Undifferentiated components from 186 pathology images of mixed-type gastric cancer were annotated using the open-source pathology imaging software QuPath. A U-Net neural network was trained to recognise, and segment differentiated components in the same images. The outcomes from QuPath and U-Net were used to calculate the ratio of differentiation/undifferentiated components which were correlated to lymph node metastasis.

Results: The models established by U-Net recognised ~91% of the regions of interest, with precision, recall, and F1 values of 90.2%, 90.9% and 94.6%, respectively, indicating a high level of accuracy and reliability. Furthermore, the receiver operating characteristic curve analysis showed an area under the cure of 91%, indicating good performance. A bell-curve correlation between the differentiated/undifferentiated ratio and lymphatic metastasis was found (highest risk between 0.683-1.03), which is paradigm-shifting.

Conclusion: QuPath and U-Net exhibit promising accuracy in the identification of undifferentiated and differentiated components in mixed-type gastric cancer, as well as paradigm-shifting prediction of metastasis. These findings bring us one step closer to their potential clinical application.

Keywords: gastric cancer, QuPath, U-Net, artificial intelligence, metastasis

Introduction

Gastric cancer remains one of the leading causes of cancer and death worldwide. According to GLOBOCAN 2020 global cancer statistics, gastric cancer contributed to 5.6% of all new cancer cases and 7.7% of all cancer-related deaths [1], which made it the fifth most common cancer and ranked the third leading cause of death worldwide [2]. East Asia has the world's highest incidence of gastric cancer, and it is the third most common new cancer case in China [3].

Gastric cancer is often in advanced stages when first detected. It has a heterogeneous nature that can present with different histological subtypes, categorised into intestinal, diffuse, and mixed types based on Lauren's criteria [4]. Each cancer type has distinct morphological and molecular features, e.g. adenoid differentiation in the intestinal type, and irregular and diffused structure in the diffuse type [4]. Mixed-type gastric cancer, in particular, is characterised by the co-existence of glandular and undifferentiated components and is associated with a more unfavourable prognosis compared to the other two subtypes. Pathological assessment of tissue specimens continues to serve as the gold standard for diagnosis, yet it heavily relies on the expertise of pathologists and their ability to accurately identify the glandular and undifferentiated components in the tissue sections.

As the precise diagnosis of mixed-type gastric cancer can be challenging due to its complex histological features and overlapping characteristics with other gastric cancer subtypes, Artificial Intelligence may have transformative potential to overcome this clinical challenge. Here, we investigated the feasibility of machine learning techniques, which have been fast developed in clinical oncology for diagnosis, predicting prognosis and informing clinical decisions [5]. The convolutional neural network is the most commonly used approach that has been implemented in cancer diagnosis using endoscopic images [6]. U-Net is one such model for image segmentation, which uses a U-shaped topology with an encoder and a decoder to extract and analyse the features of the image through convolution and pooling to generate segmentation results [7]. To date, U-Net has been widely used in developing automated medical image segmentation, especially in cancer images, with high accuracy and robustness [8, 9]; however, its application in diagnosing mix-type gastric cancer from pathological images has not been reported. On the other hand, QuPath is an open-source pathology software for image analysis, including visualisation, segmentation, classification, and quantitation [10], which has a strong potential for clinical use in the future. Therefore, we trained both QuPath and U-Net to automate the segmentation of undifferentiated and differentiated components in pathological images of mixed-type gastric cancer.

In recent years, mixed-type gastric cancer has been found to be associated with higher risks of lymph node metastasis at both early and advanced stages compared with the other two types [11, 12]. The metastatic risk may be closely related to the differentiation status of the cancer cells rather than the staging, where undifferentiated components have a higher likelihood of migrating to the lymph nodes and thereafter, remote organs [13]. The prediction of lymph node metastasis is crucial for deciding the extent of lymphadenectomy by surgeons. Insufficient lymphadenectomy may result in cancer recurrence and metastasis, whereas over-lymphadenectomy can lead to complications, such as oedema and lymphatic fistula, affecting post-operational recovery [14]. Therefore, in this study, we correlated the ratio of differentiated/undifferentiated components to lymphatic metastasis identified during surgery to determine whether this ratio is a good predictor for the risk of metastasis of mixed-type gastric cancer during treatment planning.

Subjects and Methods

Subjects

A total of 186 pathology images from 70 cases were selected from patients undergoing gastrectomy

and lymphadenectomy from September 2019 to September 2022 who were subsequently diagnosed with mixed-type gastric cancer by pathologists at the First Affiliated Hospital of Gannan Medical University. All slides were stained by hematoxylin and eosin (H&E), scanned as a whole slide image containing the entire area of the lesion (KF-PRO-005-EX, 40x mag, 0.25mm/pixel), and saved as Scalable Vector Graphics (SVS) files. The inclusion criteria were: no large area of necrosis within cancer tissue; confirmed diagnosis of mixed-type gastric adenocarcinoma by both H&E and immunohistochemistry staining; complete removal of cancer tissue; ≥ 15 lymph nodes collected from perigastric, D2 and D3 regions; and having complete admission record. The exclusion criteria were: patients receiving additional anti-cancer therapies before the surgery; low quality of the original staining and slides; and incomplete admission record.

Deep learning of mixed-type gastric adenocarcinoma

Training segmentation of regions of interest (ROI)

The differentiated components in the entire slide of a mixed-type gastric adenocarcinoma were isolated as ROI in QuPath software using the 'Create Threshold' function (circled by a red line in Figure 1a). This resulted in 13006 ROI with a total area between 122 – 47264 μm^2 (Figure 1b). U-Net architecture, including an encoding module and a decoding module, was used to segment the areas outside the ROI into small patches, which were trained together with the ROI (Figure 1c). ROI was covered by cv2.fillPoly during patch segmentation. The patch sizes were also adjusted (1028 x 1028 μm) to prevent overlapping between the ROI and non-ROI areas. The empty spaces or unoccupied areas were excluded during the analysis by setting a minimum threshold in U-Net (Figure 1d). The training also considered multiple sections in the same image during segmentation.

During the analysis of the distinguished components within the ROI using QuPath, it was observed that the presence of glandular structures exhibiting various levels of differentiation could potentially impact the accuracy of segmentation. To mitigate this issue, the aforementioned region was individually annotated, resulting in the generation of distinct categories of ROI regions. These differentiated components were subsequently exported for further analysis. Regarding the diffused poorly differentiated components in U-Net, signet ring cells and acellular mucin pools were considered poorly differentiated components. The 'Create Threshold' function also was used to distinguish cancerous cells from other cell types, such as smooth muscle, immune cells, and neurons. This process involved adjusting the threshold, which would have imposed a substantial workload if performed manually. The differences in pixel values among different cell types enable accurate identification. For example, for immune cells, the resolution was selected as full (0.27 μm/px), which can retain the original image and make the classification more accurate. The channel was selected as red, and the prefilter was selected as Gaussian. For the smooth muscle cells, which tend to have higher pixels than the undifferentiated cancer cells, lowering the threshold can exclude the muscle cells during analysis. For neurons, the Smoothing Sigma value was finely adjusted manually to exclude them from cancer cells. Smoothing Sigma value was also tuned when there was a significant variation in tumour distribution and morphology. Connective tissue and adipose tissue normally yield extremely high pixel values, and therefore did not require special settings. In some cases, a few perigastric lymph nodes were present in the outskirt of the images, which can contain undifferentiated and differentiated metastatic cancer cells. Those lymph nodes were recorded as perigastric lymph node metastases.

Deep learning

Before training the model, it is necessary to divide the dataset into a training set and a test set. The "train-test-split" function was used to separate the patch-based SVS image information from the extracted ROI regions. The training set accounted for 90% of the data, while the remaining 10% data were in the test set. Then, the U-Net model was used to train the differentiated glandular area in the SVS image and perform automatic segmentation. During the training, the setting of batch size was 4,

the learning rate was 1e-4, and the number of iterations was 50. The accuracy was improved through multiple training iterations. The U-Net model adopted the classic Convolutional Neural Networks structure, which can segment the differentiated cancer components in advanced mixed-type gastric cancer. The U-Net model constructed in this project included four downsampling paths and four upsampling paths. Each downsampling path consisted of two convolutional layers and one max-pooling layer, while each upsampling path consisted of an upsampling layer, two convolutional layers, and a ReLU activation function. The Softmax Activation function was used for the output layer. The input was the original image, and the output was the segmented result. The learning curve is shown in Figure 2.

For tissues that are difficult to distinguish, segmentation was performed through multiple comparisons to achieve the best outcome using different thresholds and Smoothing Sigma values. After determining the ROI by the Annotation function, each region was exported one by one into a .xlsx file to achieve the final threshold for training.

It is necessary to evaluate the performance of the U-Net model using the output results. The receiver operating characteristic (ROC) curve and area under the curve (AUC) value were used. The ROC curve was plotted using the correlation between the true positive and false positive rates to reflect the model performance at different thresholds. As a result, the higher the AUC value, the better the model performance.

The trained model was also subjected to model calibration. In model calibration, the un-analysed SVS images of advanced mixed-type gastric cancer (without manual annotation of ROI) were segmented following the above method using a 1024 x 1024 window. After the U-Net model was trained, the predicted image was used to evaluate the model performance.

Quantifying the ratio of differentiated/undifferentiated components in mixed-type gastric cancer
Through the model construction, differentiated and undifferentiated components were identified in advanced mixed-type gastric cancer images. All the ROI data were exported by Annotation measurements, including image information, area, and pixel coordinates. Then, the area values were used to calculate the differentiated/undifferentiated ratio (DUR). This ratio was subsequently correlated with age, gender, tumour status, and lymph node metastasis (LNM) for all 70 patients. Age, gender ("male" = 0, "female" = 1), tumour size, tumour stage, and DUR were used as independent variables, and LNM was used as a dependent variable ("no lymph node metastasis" = 0, "lymph node metastasis" = 1). A random forest model was used to evaluate the correlation between the independent and the dependent variables. Random Forest Regressor from Sklearn in the Python library was used to build the random forest model. Then the index of each variable was obtained by Feature Importance to assess whether the DUR is an independent risk factor for LNM, and compare the effect of each variation on LNM.

After confirming that the DUR is an independent risk factor for LNM, a naive Bayes classifier was used to investigate the correlation between them. DUR was divided into 20 intervals, labelled as L1 to L20. All values were converted into one-hot encoding, and interval information was converted into model input. These codings were used as feature variables for classification. The best alpha value was selected through ten-fold cross-validation, usually set to 0.1. After importing all the data, the GridSearchCV function was used to optimise the hyperparameter for training the naive Bayes classifier. The trained model was then used to predict the probability of LNM in each DUR interval. Such prediction can assist the decision-making process on the extent of lymphadenectomy.

Results
Model evaluation

Among 13006 ROI, U-Net recognised 11,822 True Positive (TP), 936 False Positive (FP), 184 False Negative (FN), and 64 True Negative (TN) results. The precision was calculated as TP / (TP + FP) = 0.9266, suggesting a strong capability of categorising. The recall was calculated as TP / (TP + FN) = 0.9847, suggesting a strong recognition ability of positive samples. The F1 score was calculated 2 x (precision x recall) / (precision + recall) = 0.9548, suggesting the model has a strong overall performance. The AUC of the ROC curve was 0.91 suggesting a good performance of U-Net (Figure 3). During model calibration, SVS images were segmented into patches without annotated ROI before the analysis using U-Net. Some differentiated components (~ 9%) were not recognised, which may be due to a small number of negative components during training.

When evaluating the recognition and segmentation of undifferentiated components, the Smoothing Sigma value was typically between 0-5, with a typical value of 2.5, while the threshold was usually between 80-200. Figure 4a shows the segmentation of normal glands and cancer tissue through threshold adjustment (same Smoothing Sigma value for the same slide), where the cancer component was labelled in red. Figure 4b shows the cancer tissue (in red) infiltrating inside muscle tissue was segmented from smooth muscle accurately. Figure 4c shows the identified undifferentiated components (in red) in the mucus of the mixed-type cancer tissue by adjusting the threshold. Using a similar method, lymphoid tissue (in blue) can be easily segmented from surrounding cancer tissue (Figure 4d).

Variable to predict the risk of LNM

The age, gender, tumour size, tumour stage, DUR and LNM information from each case are summarised in Table 1. The risk of LNM is lower before the age of 58, but increases significantly with age, indicating that LNM is more likely to occur in elderly patients (Figure 5a). The incidence of LNM in male patients was higher than in female patients (Figure 5b). The risk of LNM is the highest when the tumour diameter is between 3-5cm (Figure 5c), with a much higher risk of LNM in stage 4 than in stage 3 (Figure 5d), as expected. Also, the correlation between the DUR and the risk of LNM exhibits a bell curve, with a higher risk in the middle range (Figure 6a). Very low and very high DUR correlate with a low risk of LNM occurrence (Table 2). The likelihood of LNM reached its peak when the DUR was between 0.683 and 1.03. Figure 6b also shows that the middle value of DUR correlates with the highest lymph node metastatic ratio (the number of metastatic lymph nodes / total number of lymph nodes). These findings suggest that in advanced mixed-type gastric cancer, the fewer mixed components, the lower the risk of LNM. In summary, there is a correlation between LNM and age, gender, tumour size, tumour stage, and DUR.

Importance index of independent values

A random forest prediction model rated the importance of each parameter (Figure 7). The DUR has the highest index, suggesting the greatest impact on LNM; while gender has the smallest impact, suggesting no strong gender difference in the risk of LNM. The precision of the model was 0.79, the recall rate was 0.57, and the F1 value was 0.73, indicating a reasonable accuracy of the prediction model. With the above model, it can be determined that DUR is an independent risk factor for LNM, and the relationship between them is non-linear.

Discussion

Advanced mixed-type gastric adenocarcinoma requires accurate staging to determine the extent of the disease and the appropriate treatment plan. With the accelerated development of Artificial Intelligence, it has been increasingly used to develop reliable and accurate automated diagnostic models for tumour diagnosis based on pathological images. This approach can be advantageous in reducing errors caused by human factors. In this study, we used deep learning techniques to train U-Net and QuPath in diagnosing mixed-type gastric adenocarcinoma, which displayed good efficiency in recognising differentiated and undifferentiated components from pathology images. We also

showed that the DUR can predict the metastatic risk of such cancer type reasonably well.

While early-stage gastric adenocarcinomas can be eliminated by endoscopic procedures due to their invasion confined to the gastric mucosa and submucosa without lymph node metastasis, poorly differentiated type and late-stage cancers require resection in addition to chemotherapy and radiotherapy. Albeit the guidelines on resection procedure for gastric adenocarcinomas at different stages, the practice varies from surgeon to surgeon, and different countries have different standards too. Among them, the extent and need for lymphadenectomy continue to be debated and studied. According to the 2022 version of the resection for gastric adenocarcinomas in China [15], there are two types of lymphadenectomy, D1 (lymph nodes around the stomach, i.e. groups 1-7) and D2 (all lymph nodes in D1, and those along the hepatic artery, left gastric artery, celiac trunk, splenic artery, and splenic hilum). It is common to perform D2 in Asian countries, while D1 is a standard in Western countries [16]. However, a study has shown that there is no significant difference in 5-year survival rates between D1 and D2 lymphadenectomy [17, 18]; whereas there has been some benefit of D2 lymphadenectomy in the survival rate for late-stage patients [19]. However, an increased mortality rate may also occur after D2 lymphadenectomy.

The challenge in treating mixed-type gastric cancer in the early stage lies in whether lymphadenectomy is required when the tumour size is relatively small. Here, we showed that metastasis to nearby lymph nodes did occur in small-size tumours and patients at early stages. As such, the precise prediction of metastasis through the quantification of distinct cancer cell types can assist surgeons in making informed treatment decisions, ultimately reducing the risks of remote organ metastasis and recurrence. In previous studies, ImageJ has been commonly used to measure the areas of different cell types manually, which can be labour-intensive even with small-size early-stage cancers. This task becomes almost impossible when facing much larger size and late-stage cancers. The availability of advanced high-definition imaging methods empowers deep learning to construct diverse models and train them with data, thereby facilitating the acquisition of new data in a non-conventional manner. Here, we used U-Net neural network architecture based on fully convolutional networks. The additional modifications make it suitable for image segmentation tasks [20, 21]. This system can complement the complex operational skill needed for QuPath, albeit the coding for QuPath is openly available [22]. However, U-Net is more efficient in segmenting structured and relatively standardised components, while the QuPath software demonstrates superior adaptability in handling various scenarios.

The most important segmentation aspect is to distinguish between cancerous and immune cells. It can be difficult to achieve by a simple threshold adjustment. In such a scenario, the threshold can be adjusted to select all tissues except muscle and fibre tissues, followed by the indirect calculation of cancer tissue by filtering out immune cells and normal tissue with similar pixel values. Nevertheless, this situation is relatively rare; in most cases, cancer tissue can be readily identified.

The findings presented in this paper have unveiled a significant paradigm shift, which is the bell curve correlation between the DUR and the risk of LNM. Future studies need to investigate the mechanisms underlying this correlation in mixed-type gastric cancer, which may suggest new markers for early diagnosis, treatment targets or post-treatment surveillance. Artificial Intelligence-based automated cancer diagnostic models can rapidly and accurately analyse large volumes of data, providing clinicians with more comprehensive information within shorter time frames, thereby reducing waiting times for patients, particularly during surgical procedures. This can also support precision medicine, assisting the development of a personalised treatment plan tailored to an individual's needs, leading to improved survival rates.

Conclusion

The utilisation of an automated diagnostic model combining QuPath and U-Net holds the potential to enhance the precision and efficiency of diagnosing and predicting the prognosis of mixed-type gastric cancer. The significance of our findings brings us closer to incorporating such technology into routine clinical practice. By enabling clinicians to make more informed treatment decisions, this advancement has the potential to improve patient outcomes significantly.

Author Contributions

Conceptualisation, D.L., Y.H.; methodology, R.L.; formal analysis, R.L.; investigation, X.N., R.L., N.W., X.X., S.W., Y.W.; writing - original draft preparation, X.N., H.C.; writing - review and editing, R.L., D.L., Y.H., H.C.; supervision, Y.H., C.Y., D.L.; funding acquisition, C.Y. All authors have read and agreed to the submitted version of the manuscript.

Funding

This work was supported by grants from the National Natural Science Foundation of China (81971309 and 32170980), Guangdong Basic and Applied Basic Research Foundation (2022B1515020012), and Shenzhen Fundamental Research Program (JCYJ20210324123212035, RCYX20200714114644167, and ZDSYS20220606100801003).

Declaration of interests

The authors have no competing interests to declare in relation to this work.

References

[1] Sung H, Ferlay J, Siegel R L, et al. Global Cancer Statistics 2020: GLOBOCAN Estimates of Incidence and Mortality Worldwide for 36 Cancers in 185 Countries [J]. CA Cancer J Clin, 2021, 71(3): 209-49.

[2] Ajani J A, D’ amico T A, Bentrem D J, et al. Gastric Cancer, Version 2.2022, NCCN Clinical Practice Guidelines in Oncology %J Journal of the National Comprehensive Cancer Network [J]. 2022, 20(2): 167-92.

[3] Xia C, Dong X, Li H, et al. Cancer statistics in China and United States, 2022: profiles, trends, and determinants [J]. Chin Med J (Engl), 2022, 135(5): 584-90.

[4] Berlth F, Bollschweiler E, Drebber U, et al. Pathohistological classification systems in gastric cancer: diagnostic relevance and prognostic value [J]. World J Gastroenterol, 2014, 20(19): 5679-84.

[5] Swanson K, Wu E, Zhang A, et al. From patterns to patients: Advances in clinical machine learning for cancer diagnosis, prognosis, and treatment [J]. Cell, 2023, 186(8): 1772-91.

[6] Hirasawa T, Aoyama K, Tanimoto T, et al. Application of artificial intelligence using a convolutional neural network for detecting gastric cancer in endoscopic images [J]. Gastric Cancer, 2018, 21(4): 653-60.

[7] Ronneberger O, Fischer P, Brox T. U-Net: Convolutional Networks for Biomedical Image Segmentation; proceedings of the Medical Image Computing and Computer-Assisted Intervention – MICCAI 2015, Cham, F 2015//, 2015 [C]. Springer International Publishing.

[8] Yin X-X, Sun L, Fu Y, et al. U-Net-Based Medical Image Segmentation [J]. J Healthc Eng, 2022, 2022: 4189781.

[9] Wang X, Chen Y, Gao Y, et al. Predicting gastric cancer outcome from resected lymph node histopathology images using deep learning [J]. Nat Commun, 2021, 12(1): 1637.

[10] Bankhead P, Loughrey M B, Fernández J A, et al. QuPath: Open source software for digital pathology image analysis [J]. Sci Rep, 2017, 7(1): 16878.

[11] Horiuchi Y, Ida S, Yamamoto N, et al. Feasibility of further expansion of the indications for endoscopic submucosal dissection in undifferentiated-type early gastric cancer [J]. Gastric Cancer, 2020, 23(2): 285-92.

[12] Lu H, Sun Y, Zhu Z, et al. Differentiated/undifferentiated mixed type is a prognostic factor for T2/T3 gastric cancer patients [J]. Expert Rev Gastroenterol Hepatol, 2021, 15(11): 1329-36.

[13] Takeuchi H, Abe N, Hashimoto Y, et al. Establishment of pathological quantitative method for determining undifferentiated component ratio in patients with differentiated/undifferentiated mixed-type early gastric cancer and clinical significance of this ratio [J]. Gastric Cancer, 2018, 21(4): 661-71.

[14] Li Z, Bai B, Zhao Y, et al. Severity of complications and long-term survival after laparoscopic total gastrectomy with D2 lymph node dissection for advanced gastric cancer: A propensity score-matched, case-control study [J]. Int J Surg, 2018, 54(Pt A): 62-9.

[15] Health Commission of the People's Republic of China N. National guidelines for diagnosis and treatment of gastric cancer 2022 in China (English version) [J]. Chin J Cancer Res, 2022, 34(3): 207-37.

[16] Coburn N, Cosby R, Klein L, et al. Staging and surgical approaches in gastric cancer: a clinical practice guideline [J]. Current oncology (Toronto, Ont), 2017, 24(5): 324-31.

[17] Uslu A, Zengel B, İlha E, et al. Survival outcomes after D1 and D2 lymphadenectomy with R0 resection in stage II-III gastric cancer: Longitudinal follow-up in a single center [J]. Turkish journal of surgery, 2018, 34(2): 125-30.

[18] Schmidt B, Yoon S S. D1 versus D2 lymphadenectomy for gastric cancer [J]. Journal of surgical oncology, 2013, 107(3): 259-64.

[19] Faiz Z, Hayashi T, Yoshikawa T. Lymph node dissection for gastric cancer: Establishment of D2 and the current position of splenectomy in Europe and Japan [J]. Eur J Surg Oncol, 2021, 47(9): 2233-6.

[20] Falk T, Mai D, Bensch R, et al. U-Net: deep learning for cell counting, detection, and morphometry [J]. Nat Methods, 2019, 16(1): 67-70.

[21] Lalonde R, Xu Z, Irmakci I, et al. Capsules for biomedical image segmentation [J]. Med Image Anal, 2021, 68: 101889.

[22] Berben L, Wildiers H, Marcelis L, et al. Computerised scoring protocol for identification and quantification of different immune cell populations in breast tumour regions by the use of QuPath software [J]. Histopathology, 2020, 77(1): 79-91.

Tables

Table 1: Case information

ID	Age	Gender	Tumor size	Tumor stage	LNM	DUR
1	49	1	2.0	4	1	80.0000
2	59	1	1.5	4	0	0.5000
3	64	0	1.8	4	1	9.5509
4	72	1	2.5	3	1	0.2585
5	73	1	3.0	3	0	0.0190
6	64	0	4.5	4	1	9.5112
7	50	0	8.0	4	1	7.5980
8	67	0	3.0	4	1	0.3366
9	74	1	3.0	4	1	1.8992
10	75	1	4.0	4	1	9.6487
11	75	0	4.0	4	1	5.2703
12	73	1	5.0	4	1	131.0717
13	71	0	1.5	3	0	2190.3160
14	68	0	4.5	4	1	2060.9830
15	66	1	2.0	4	0	0.1336
16	58	0	5.0	4	1	0.2459
17	63	1	1.0	3	1	1.6882
18	53	0	3.5	4	1	5.7361
19	62	0	3.4	4	1	0.5412
20	29	1	7.0	4	1	7.5846
21	67	1	7.0	4	1	0.9231
22	74	0	2.0	4	1	0.2350
23	49	1	7.0	3	0	0.1666
24	50	0	5.5	4	1	0.2070
25	52	1	4.0	4	0	978.0299
26	70	0	5.0	4	1	6.7684
27	66	1	3.0	4	1	0.4571
28	62	0	7.0	4	1	0.4519

29	67	1	7.0	4	0	2168.7980
30	66	0	3.0	4	1	0.7827
31	70	0	3.4	4	1	0.2444
32	68	0	3.0	4	0	0.1509
33	39	1	5.0	4	1	0.3565
34	48	1	5.5	4	1	2.2289
35	45	0	2.5	3	0	0.1250
36	64	0	7.5	4	1	0.5740
37	59	0	2.0	4	1	2275.9250
38	72	0	3.0	4	1	0.3562
39	63	0	6.5	4	0	2494.9110
40	68	0	3.5	4	1	1775.3960
41	61	0	2.5	4	0	0.1153
42	65	0	4.0	4	1	5.3192
43	65	0	2.5	3	1	0.3883
44	61	0	3.5	4	0	2199.1930
45	62	0	2.0	4	1	0.3394
46	81	0	1.0	4	0	0.1374
47	52	0	8.0	4	1	2.2020
48	59	0	4.0	4	1	2.9745
49	68	0	2.5	4	0	2050.1630
50	56	1	3.0	4	1	11290.0000
51	65	1	5.0	4	1	0.3327
52	64	0	5.0	4	1	1.3638
53	68	0	3.0	4	1	1570.0740
54	72	0	8.5	4	1	0.3762
55	47	1	2.2	4	1	5.2038
56	70	1	3.0	4	1	0.6794
57	55	1	8.0	4	0	2577.2910
58	53	0	3.0	4	0	0.2765
59	75	0	3.5	4	1	2207.1190

60	57	0	5.0	4	1	0.3062
61	61	0	4.0	4	1	5.2319
62	58	1	3.5	4	1	170.2422
63	59	0	2.5	4	1	0.7517
64	59	0	4.0	4	1	0.4855
65	73	0	4.0	4	1	6.5969
66	73	0	2.5	4	0	0.2920
67	65	1	7.0	3	0	0.1970
68	39	1	3.0	4	1	1.1375
69	65	0	2.5	4	1	0.6689
70	67	0	5.5	4	0	0.1896

Gender: "male" = 0, "female" = 1; LNM: "no lymph node metastasis" = 0, "lymph node metastasis" = 1. DUR: the differentiated/undifferentiated ratio; LNM: lymph node metastasis.

Table 2: Risk of LNM based on the DUR interval

L	DUR interval	Risk probability
L1	DUR_interval_[0.019, 0.135]	0.0105
L2	DUR_interval_[0.135, 0.187]	0.0357
L3	DUR_interval_[0.187, 0.238]	0.7105
L4	DUR_interval_[0.238, 0.273]	0.7885
L5	DUR_interval_[0.273, 0.334]	0.8311
L6	DUR_interval_[0.334, 0.356]	0.8885
L7	DUR_interval_[0.356, 0.453]	0.8885
L8	DUR_interval_[0.453, 0.525]	0.8785
L9	DUR_interval_[0.525, 0.683]	0.9105
L10	DUR_interval_[0.683, 1.03]	0.9205
L11	DUR_interval_[1.03, 1.889]	0.9185
L12	DUR_interval_[1.889, 3.866]	0.9105
L13	DUR_interval_[3.866, 5.312]	0.5347
L14	DUR_interval_[5.312, 7.013]	0.6374
L15	DUR_interval_[7.013, 9.541]	0.6311
L16	DUR_interval_[9.541, 138.906]	0.6885
L17	DUR_interval_[138.906, 1703.533]	0.5885
L18	DUR_interval_[1703.533, 2170.95]	0.4105
L19	DUR_interval_[2170.95, 2244.962]	0.3105
L20	DUR_interval_[2244.962, 11290.0]	0.0885

DUR: the differentiated/undifferentiated ratio; LNM: lymph node metastasis.

Figures

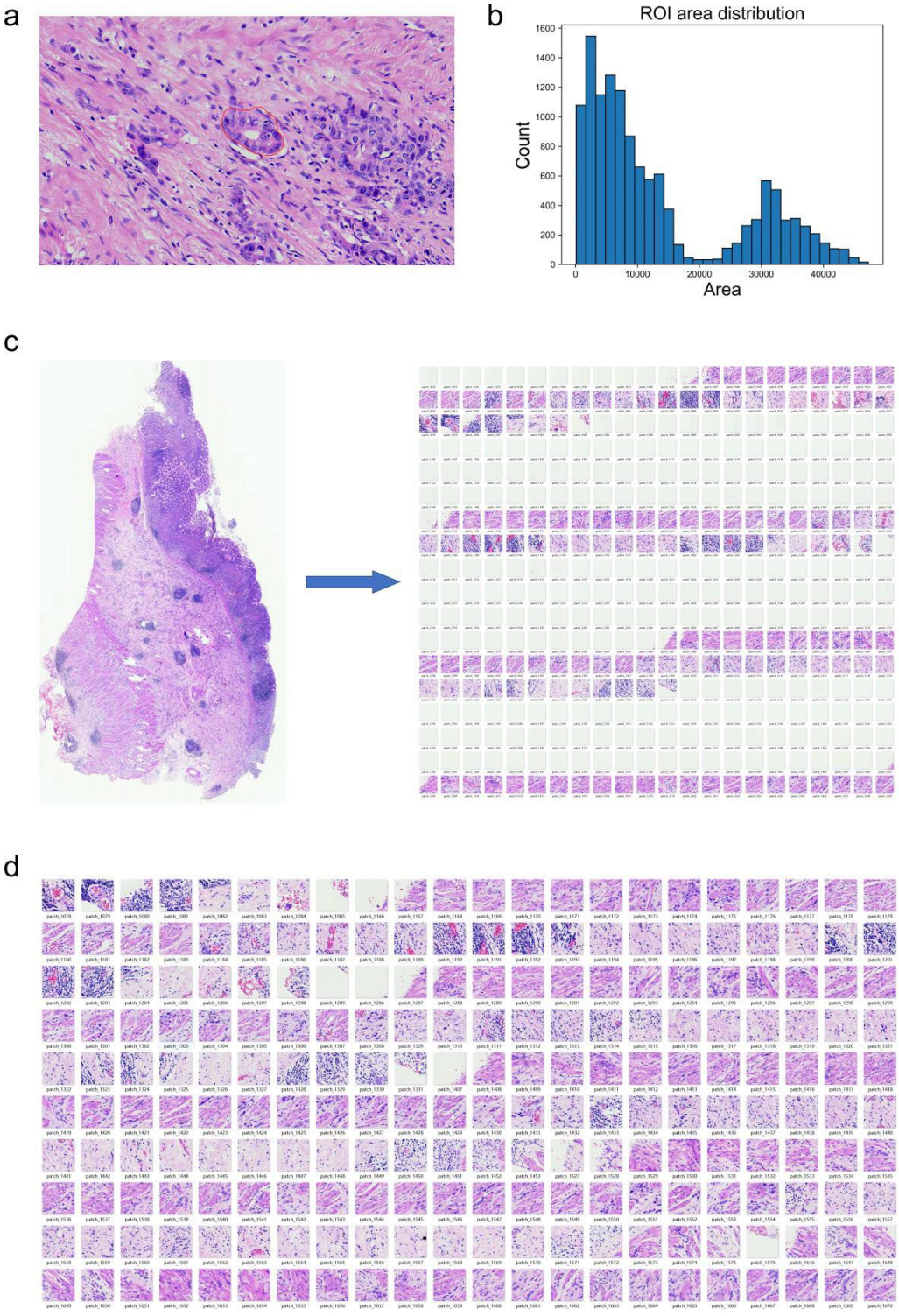

Figure 1: Representative images of segmentation of ROI. The differentiated component inside mixed-type gastric cancer tissue is idsolated using a red-solid line which is surrounded by undifferentiated components (poorly differentiated adenocarcinoma) (a). Distribution of ROI areas in all slides (b). Representative images of segmentation of non-ROI areas into patches (c) and re-adjust to better exclude the empty areas (d). ROI: region of interest.

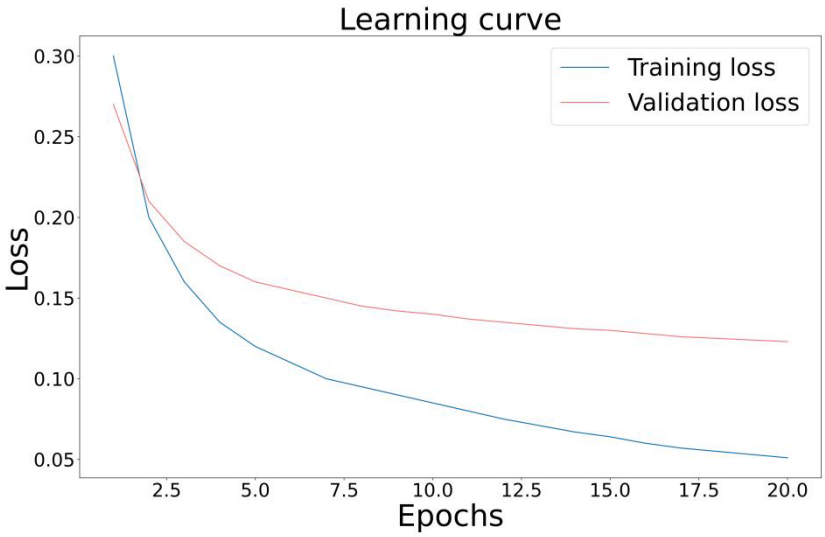

Figure 2: The learning curve of the U-Net model.

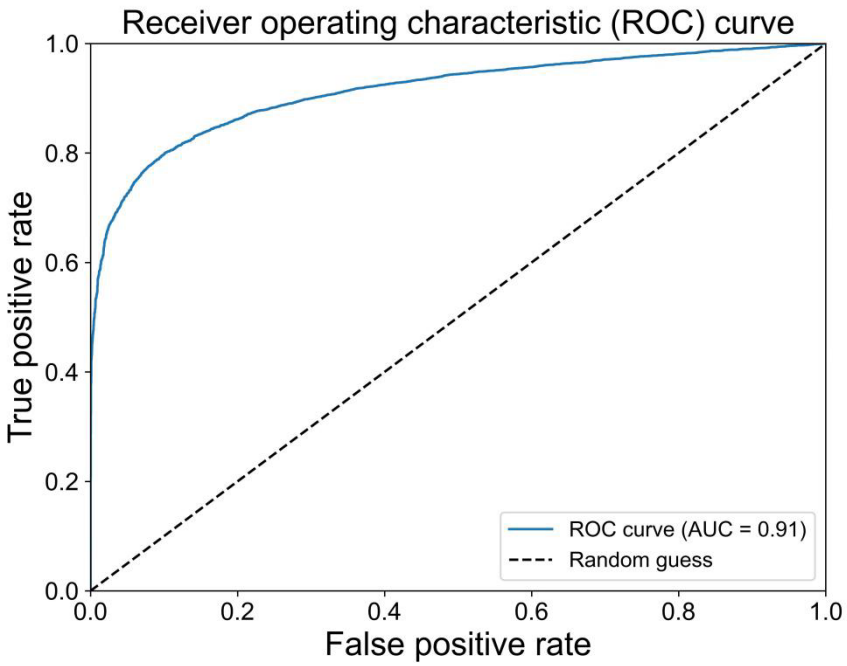

Figure 3: The AUC of the ROC curve. AUC: area under the curve; ROC curve: the receiver operating characteristic curve.

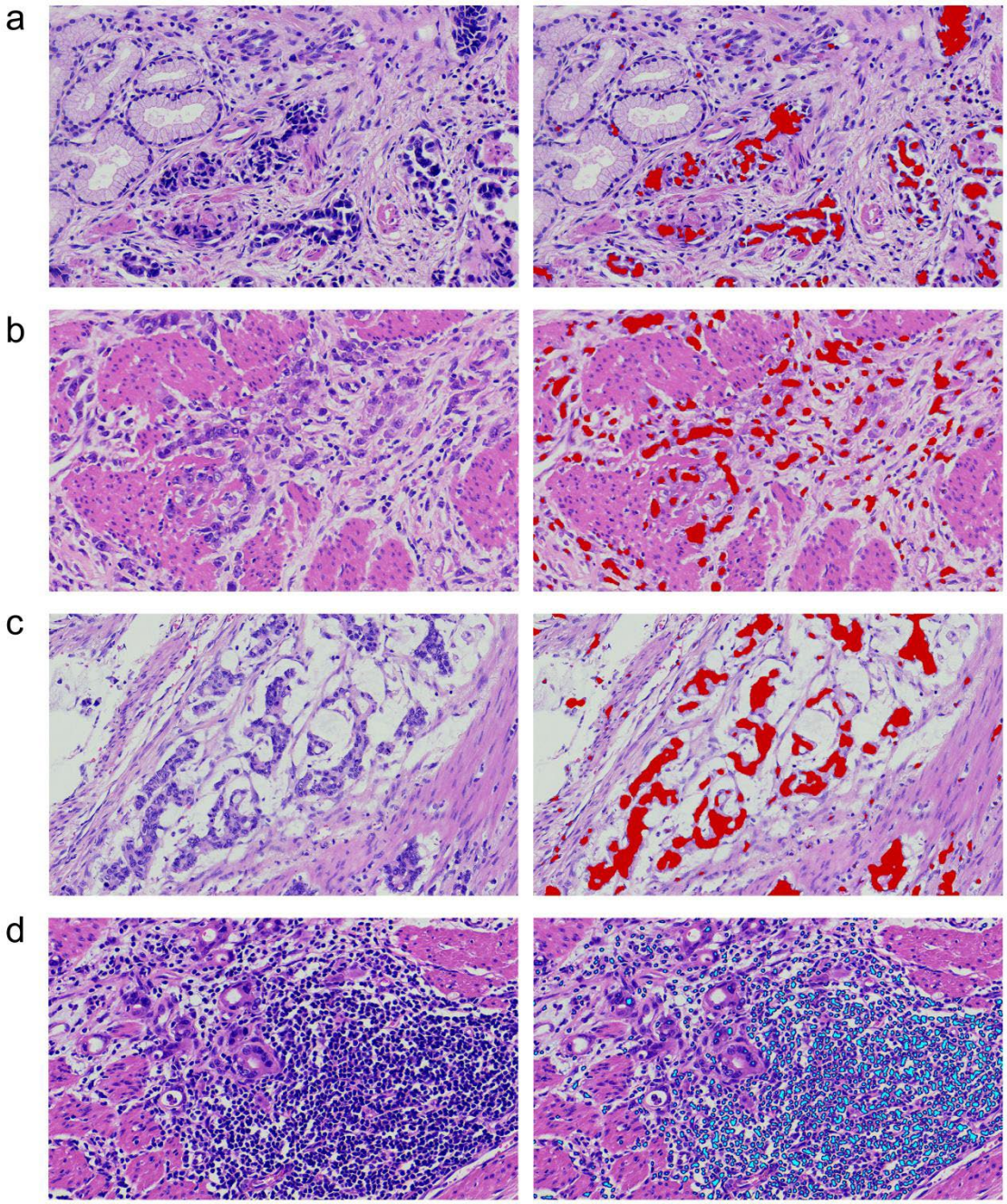

Figure 4: Segmentation of normal tissue and cancer tissue (red: cancer tissue, a), smooth muscle and cancer tissue (red: cancer tissue, b), undifferentiated components (red) in cancer tissue (c), and lymphoid tissue (blue) inside the cancer tissue (d).

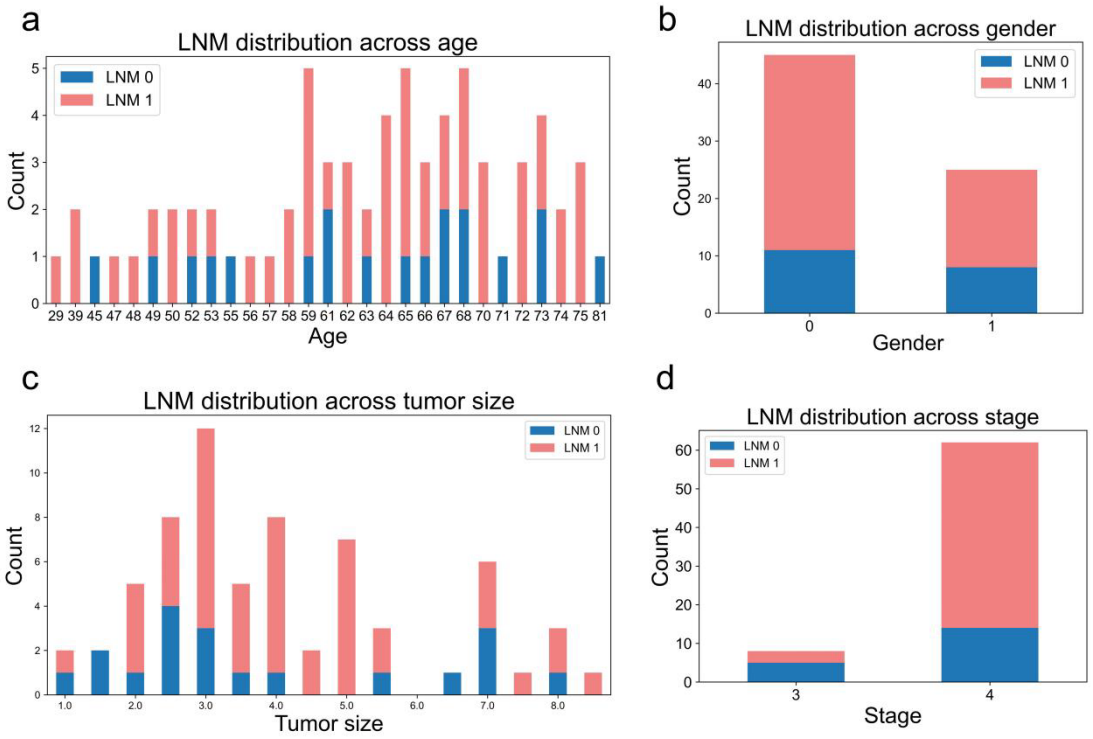

Figure 5: Risk of LNM across age (a), gender (b), tumour size (c), tumour stage (d). Gender: "male" = 0, "female" = 1; LNM: "no lymph node metastasis" = 0, "lymph node metastasis" = 1. LNM: lymph node metastasis.

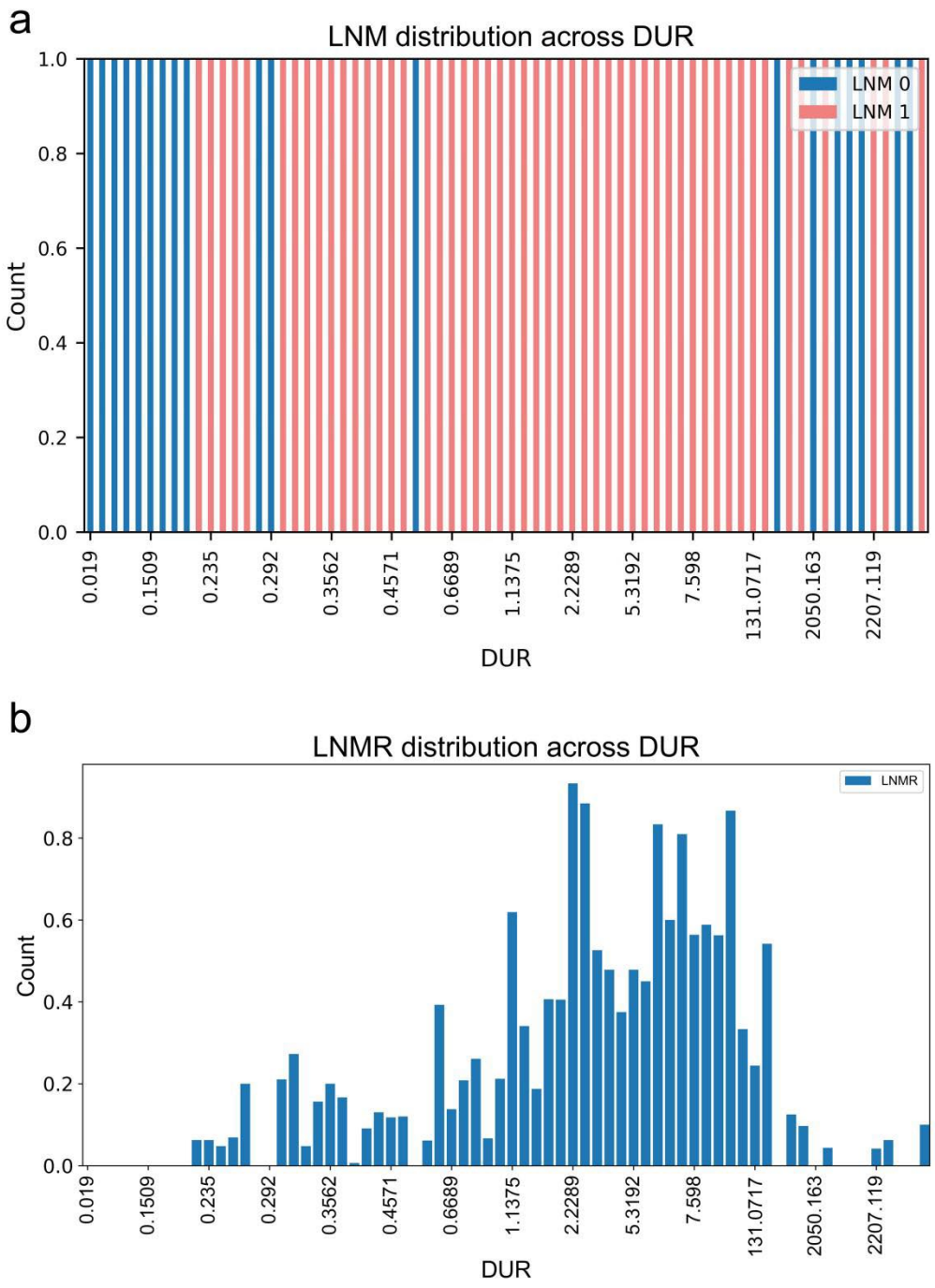

Figure 6: The correlation between LNM and DUR. (a) the risk of LNM across DUR, (b) the LNMR value across DUR. DUR: the differentiated/undifferentiated ratio; LNM: lymph node metastasis; LNMR: lymph node metastatic ratio (each bar representing a case).

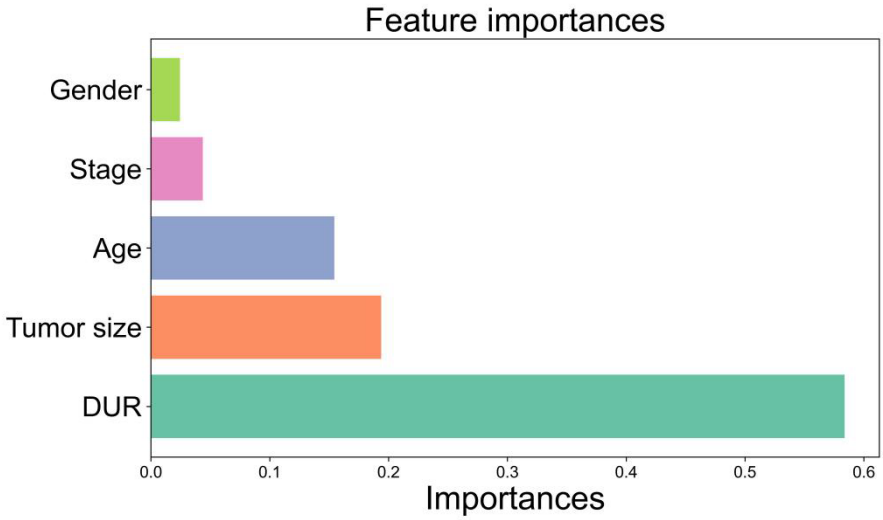

Figure 7: The index of the importance for each parameter rated by a random forest prediction model.

DUR: the differentiated/undifferentiated ratio.